Theory of size-dependent resonance Raman intensities in InP nanocrystals

J. J. Shiang, R. H. Wolters, and J. R. Heath
Molecular Design Institute, Lawrence Berkeley Laboratory and UCLA, Department of Chemistry and Biochemistry, 405 Hilgard Ave. Los Angeles, California 90095-1569

(Received 4 December 1996; accepted 3 March 1997)

The resonance Raman spectrum of InP nanocrystals is characterized by features ascribable to both longitudinal (LO) and transverse (TO) optical modes. The intensity ratio of these modes exhibits a strong size dependence. To calculate the size dependence of the LO and TO Raman cross sections, we combine existing models of Raman scattering, the size dependence of electronic and vibrational structure, and electron vibration coupling in solids. For nanocrystals with a radius >10 Å, both the LO and TO coupling strengths increase with increasing radius. This, together with an experimentally observed increase in the electronic dephasing rate with decreasing size, allows us to account for the observed ratio of LO/TO Raman intensities. © *1997 American Institute of Physics.* [S0021-9606(97)00222-5]

I. INTRODUCTION

Chemical control over the size or shape of a nanoscale crystal permits modification of its electronic and vibrational properties. Such size- and shape-dependent phenomena have been the subject of extensive physical characterization.[1] In one such class of experiments, i.e., resonance Raman spectroscopy, the motion of the lattice is used to probe not only the vibrational frequencies of the lattice but also how the electronic properties of the crystallite are modified by the displacement of the nuclear cores. Different vibrational modes, due to the presence or absence of an accompanying electric field, modulate the electronic properties on different length scales. In the well-studied II–VI class of nanocrystals, only a single mode, the longitudinal optical (LO) phonon, is observed in the resonance Raman spectrum.[2–5] Recently, it has become possible to prepare and to study size selected nanocrystallites of the more covalent III–V semiconductor material, InP.[6] For this material, both the LO and the transverse optical (TO) phonon modes are observed and the ratio of their intensities is strongly correlated to nanocrystal size.[7] This paper is devoted to a detailed explanation of this size dependence.

In a bulk polar solid, the optical modes split into two distinct branches, the LO and the TO modes. Both modes distort the unit cell in the same way, which can be visualized as the central atom of a tetrahedron moving relative to the four other atoms (Fig. 1, Col. I). When there is a difference in effective charge of the two atoms, a local polarization is generated. The modes differ in the alignment of this charge displacement between different unit cells. Thus the polarization fields that result from excitation along either of the mode coordinates are different. The polarization field induced by the LO mode is curl-less, has a finite divergence, and generates a macroscopic electric field which exhibits long-range coupling to the motion of the electrons. The TO mode, on the other hand, produces a polarization field which is divergence-less and has net curl. Therefore, no macroscopic electric field is produced, and the electron–phonon coupling is relatively short range.

For metals and semiconductors, one can reduce the crystallite size to near molecular length scales while maintaining a bulklike local bonding geometry about an atom located in the interior of the crystallite. Thus despite the large numbers of atoms involved, the underlying structural regularity of a nanocrystal makes it possible to extend semi-empirical models of infinite solids, such as tight binding and k^*p, to finite size. The adjustable parameters in these models correspond to bonding interactions between neighboring atoms. For the TO mode, we will be concerned with the effect that nuclear displacements have on the local (near the displacement) electronic structure of the nanocrystal. Within a unit cell, such displacements modify the parameters which couple orbitals on different atoms; e.g., bonds which are extended lead to less orbital coupling; bonds which are compressed exhibit increased coupling. Using a tight binding model, Harrison has proposed that these orbital–orbital interactions scale as $(\text{distance})^{-2}$, and it is thus possible to generate band structures not only for equilibrium bond lengths, but for displaced ones as well.[8] The modification of the band structure due to motion along an optical phonon coordinate is described by a single parameter, the optical deformation potential, d_0. This parameter can be obtained using tight binding or pseudopotential theory, and we use it to compute the TO Raman cross sections.[9]

For the LO modes, it is helpful to consider the following analogy. When an excess charge (an electron, for example) is placed in a drop of polar solvent, the solvent will distort around the charge, creating a polarization cloud which stores energy in the solvent. For a fairly large drop, the amount of solvation is independent of drop size. As the drop radius becomes comparable to the size of the polarization cloud, one expects the amount of energy deposited into the solvent to decrease for two reasons. The first is a classical effect. The amount of dielectric is reduced, and thus there is less energy to store in the medium. The second is quantum mechanical in origin. As the drop is made smaller, the electron becomes more localized and has higher kinetic energy. This makes it harder for the lattice to couple effectively to the charge. In a liquid drop, the calculation of these solvation effects requires

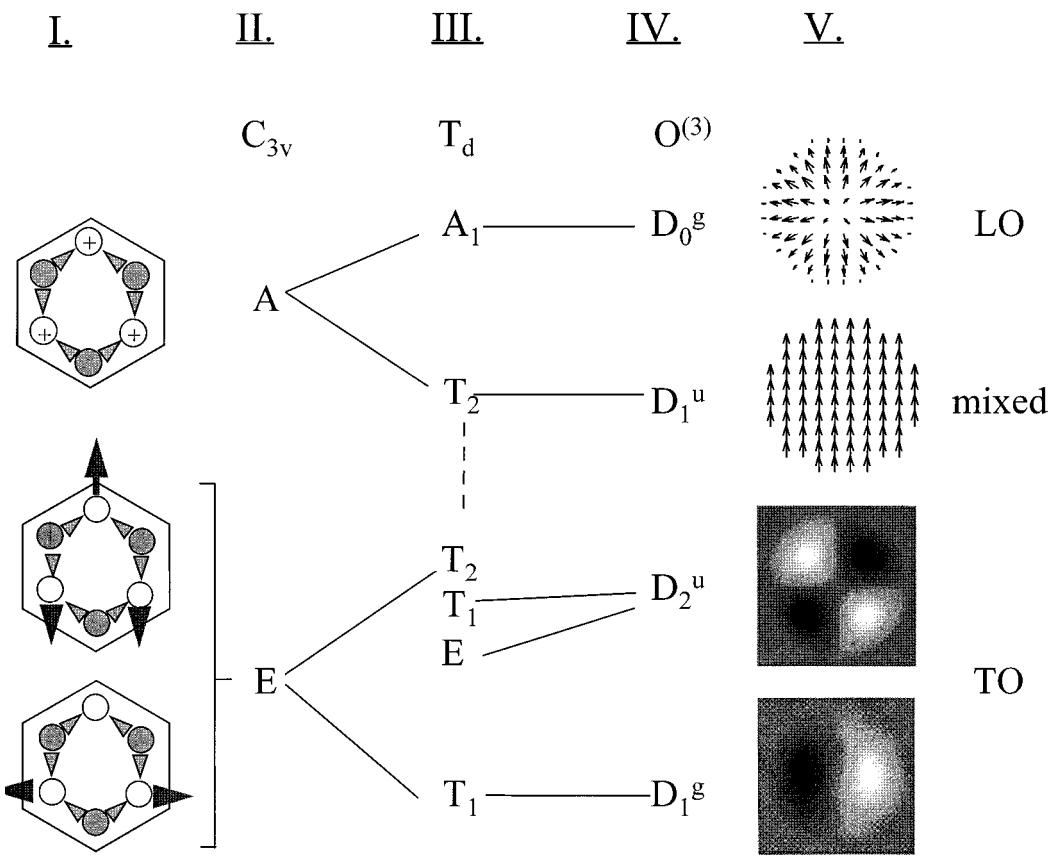

FIG. 1. Group theory correlation table which connects the symmetry labels of optical phonons to the limiting shapes of nanocrystals. Column I illustrates the mode displacements for one section of a plane in a zinc-blende lattice. Column II indicates the symmetry of each type of planar vibration. When these C_{3v} planes are arranged in a tetrahedral manner, A and E modes each give rise to different vibrational modes of the tetrahedron (Column III). Column IV shows the symmetry labels for these vibrations in the spherical case. Column V illustrates these spherical modes. The arrows for the LO and mixed mode indicate the relative motion of one sublattice relative to another. The light and dark areas for the TO mode indicate relative motion in and out of the plane.

serious computational effort.[10] For a polar crystalline solid, however, the regularity of the structure makes calculations of ''polaron'' effects relatively simple. One can, in fact, use the electron effective mass, m_e^*, to compute the effective polaron radius R_p^e:[11]

$$R_p = \sqrt{\frac{\hbar}{2m_e^*\omega}}. \tag{1}$$

The LO frequency (ω) is the mode along which solvation of the excess charge takes place. In the case where there are two polarons of opposite charge, the situation is much more complicated, as there are now four relevant length scales: the radii of the polarons, the radius of the drop, and the exciton radius. The exciton radius depends on the magnitude of the screened Coulomb potential. The situation is further complicated because the magnitudes of the polarization clouds which screen the electron and hole from each other depend on the relative motion of the charges. Fortunately, it is often the case that these various length scales are sufficiently different that only two of them are important at any given time. For InP, the Coulomb interaction between the electron and the hole is quite weak, and the exciton radius is therefore large ($\sim$140 Å). For sizes significantly smaller than this (the strong confinement regime), we can, to a first approximation, assume that the motion of the electron and the hole are uncorrellated. The polaron radii, on the other hand, are much smaller: 8 Å for the hole[17] (R_p^h) and about 33 Å for the electron (R_p^e), implying that polaronic effects continue well past the point where the Coulomb interaction dominates the relative motion of the charge carriers. This argument implies that as the lattice size is reduced well below the bulk exciton radius, the electrostatic coupling of the charge carriers to the lattice will decrease dramatically. For the LO mode, good models exist which describe the analytic limits of both very small ($\ll R_p^h$) and very large (bulk) behavior. What we need, then, is a model which allows us to connect these two limits and therefore make predictions about nanocrystals. Pullman and Buttner have developed a theory which allows for ''state-dependent'' lattice contributions to dielectric screening.[13] This theory is readily extended to finite sized crystals, and allows us to effectively connect the large- and small-size limits, and calculate size-dependent Raman cross sections for the LO modes.

This paper proceeds as follows. Over the next three sections (II–IV), a group theory formalism for discussing the vibrations of a particle in finite size is developed, and the

necessary background material for carrying out the Raman intensity calculations is covered. Confined phonon wave functions are discussed in Sec. II and confined electronic states are discussed in Sec. III. In Sec. IV an outline of the relationship between the vibration induced coupling of two electronic states and the Raman intensity is presented. In Sec. V the results from Secs. II–IV are brought together to calculate the size dependence of the TO Raman cross section. In Sec. VI we extend Pollman–Buttner's model to calculate the size dependence of the LO mode cross section. Finally, we use all of our results from Secs. II–VI to calculate the relative Raman cross section versus size and briefly discuss some of the approximations in our model.

II. OPTICAL VIBRATIONS IN FINITE SIZE: SYMMETRY CONSIDERATIONS

In this section we will utilize the formalisms of group theory to connect the LO and TO modes of a bulk zinc-blende crystal to the vibrational modes in a finite sized crystal. This will allow us to predict not only which modes are Raman allowed, but also which modes will be polarized.

There exist several theoretical treatments of the confined optical modes of a sphere.[4,14,15] Roca and co-workers have extended the electromagnetic description of the lattice vibrations to include the mechanical boundary conditions which require the mechanical displacement to vanish at the surface of the crystallite.[16] Their solutions can be divided into three classes. One class contains the modes which have ''mixed'' character, i.e., they contain polarization components both perpendicular and parallel to the radial vector ($\mathbf{r}$) from the sphere center. These modes have the following frequency in the limit of large spheres:

$$\omega^2=\omega_{\mathrm{TO}}^2\,\frac{\epsilon_0^1 l+\epsilon_0^2(l+1)}{\epsilon_\infty^1 l+\epsilon_\infty^2(l+1)}\quad \text{for } R\to\infty;\ D_1^u,D_2^g,\ldots\ . \tag{2}$$

ω is the frequency of the mode in the sphere, ω_{TO} is the bulk TO frequency at zone center, and ϵ_0, ϵ_∞ are the static and optical dielectric constants for the crystallite and the dielectric medium which surrounds it, respectively. l is the angular momentum quantum number. The notation ($D_n^{g,u}$) following the semicolon are labels of the representations from the rotation group $O^{(3)}$ to which the lowest two modes correspond, the subscript, n, corresponds to the angular momentum quantum number. If one includes the effect of the mechanical boundary conditions, these modes have a mathematically complicated shape. In the absence of these conditions, one finds that the lowest order mode, $l=1$, corresponds to a uniform translation of one sublattice (e.g., In) relative to another (e.g., P). (Fig. 1, Col. V, ''mixed'').

For $l=0(D_0^g)$, the frequency of the vibrational mode is governed by the following equation:

$$\omega^2=\omega_{\mathrm{LO}}^2+\beta_L^2\left(\frac{\nu_n}{R}\right)^2;\ D_0^g. \tag{3}$$

β_L is the dispersion of the LO mode in the bulk, and ν_n is determined by the mechanical boundary conditions. This mode is relatively simple in structure and the amplitude is given by:

$$\delta_{\mathrm{LO}}(r,\Omega)=C_n j_1\left(\nu_n\,\frac{r}{R}\right)Y_0^0(\Omega). \tag{4}$$

$Y_0^0(\Omega)$ is zeroth order spherical harmonic and a function of θ, ϕ (here represented as Ω) j_1 is the spherical Bessel function of order 1. C_n, the normalization factor, is determined by the requirement that:

$$\begin{aligned}&\frac{1}{2}\,\hbar\omega=\frac{1}{2}\,nM\omega^2C_n^2R^3I_{1n},\\ &n=\frac{4}{a^3},\\ &I_{mn}=\int_0^1 j_{m1}^2(\nu_n r)r^2\,dr,\\ &M=\frac{M_{\mathrm{In}}M_{\mathrm{P}}}{M_{\mathrm{In}}+M_{\mathrm{P}}}.\end{aligned} \tag{5}$$

Here n is the number density of oscillators (4 per zinc-blende unit cell), a is the zinc-blende unit cell parameter, M is the reduced mass of the unit cell, $M_{\mathrm{In,P}}$ are the individual nuclear masses, ω is the frequency, and R is the radius. Equation (5) results from the fact that the potential energy at maximum displacement is equal to the zero point energy and hence the amplitude at any given site is proportional to $1/R^{3/2}$. These modes are the radial breathing of one sublattice relative to another. (Fig. 1, ''LO'')

Finally there are modes which have no radial component, and the nuclear displacements are entirely tangential to the surface of the sphere:

$$\omega^2=\omega_{\mathrm{TO}}^2+\beta_T^2\left(\frac{\nu_n}{R}\right)^2;\ D_1^g,D_2^u. \tag{6}$$

β_T is the dispersion of the TO mode in the bulk, and R is the radius of the crystallite. These modes generate the following displacement field:

$$\delta_{\mathrm{TO}}(r,\Omega)=-iC_n j_l\left(\nu_n\,\frac{r}{R}\right)\left(\frac{\mathbf{L}Y_l^m(\Omega)}{\sqrt{l(l+1)}}\right), \tag{7}$$

where $\mathbf{L}$ is the angular momentum operator, Y_l^m is a spherical harmonic, and C_n, the normalization constant, is found in a manner identical to that of the LO modes. This mode corresponds to torsional motion of one sublattice relative to another (Fig. 1, Col. V, TO).

In the group $O^{(3)}$, the Raman active modes transform as D_0^g and D_2^g and thus, one expects to observe only LO and mixed type modes and not modes which have frequencies similar to the bulk TO mode (Fig. 1, Col. IV). However, these selection rules need to be modified in the case of a tetrahedral material which lacks inversion symmetry. The tetrahedral bonding of the crystal effects not only the local vibration within each unit cell, but through Wolff construc-

tion, should manifest itself in the overall shape of the crystallite. Thus in order to determine the appropriate selection rules for our crystallites, we construct a correlation table to go from the full rotation group to the tetrahedral group T_d as shown in Fig. 1.

We find that D_2^u modes decompose into a Raman active E component and a nonactive T_1 mode, suggesting that it is possible to observe TO-type modes. It also possible to go the other way, i.e., from tetrahedral symmetry to spherical. A tetrahedral crystallite consists of a series of ''shells,'' each of which has T_d symmetry. Each ''shell'' of crystallite can be divided into four ''faces'' which have C_{3v} symmetry (Fig. 1, Col. I). We shall define optical modes as consisting of two types, motions perpendicular to the plane of the shell which transform as the A_1 representation of C_{3v} and motions parallel to the plane, which transform as the E representation (Cols. I and II). We can use these two different type of motions as basis functions, and operate on them using the symmetry operations of the point group T_d. The perpendicular motions transform as A_1+T_2, while the parallel motions transform as T_1+T_2+E (Fig. 1, Col. III). By symmetry, the A_1 modes do not mix with the parallel motions and thus are purely ''radial,'' but T_2 modes derived from the perpendicular and parallel motions will mix. The T_1 and E modes remain purely parallel. These symmetry labels predict that the LO mode (A_1, D_0^g) will be strongly polarized and the TO (E, T_2, D_2) modes will be depolarized. Near resonance, the T_2 mixed modes might exhibit large depolarization ratios, due to the asymmetric nature of the Raman scattering tensor (see Mortesen and Hassing).[17] However, inhomogeneously broadened size distributions, and the large peak widths that characterize the Raman spectra of finite sized particles, may make this effect difficult to observe experimentally. These mixed modes have been assigned the moniker of ''surface modes'' in finite sized GaP[18] and CdSe[5] crystals.

III. ELECTRONIC STATES IN FINITE SIZE

For any calculation of the resonance Raman cross sections of semiconductor nanocrystals, one needs a good description of the electronic states that describe the e^- and h^+ energy levels. Conceptually, the simplest approach is to utilize a linear combination of atomic orbitals (LCAO). If one starts from individual atoms, this approach is the tight binding method, and if one starts from a bulk, periodic lattice, this approach is the $\mathbf{k}^*\mathbf{p}$ method. The physical parameters which characterize both methods are thus closely related. In this section, we will present existing literature results which extend $\mathbf{k}^*\mathbf{p}$ to finite size, and give us the appropriate envelope wave functions for describing the electron and hole states. Overall, this method is less rigorous than the tight-binding approach (for a nanocrystal) developed by Hill and Whaley,[19] but it does lead to analytic solutions for the electronic states of a spherical nanocrystal.[20–22] This method has been utilized with some success to describe various photophysical phenomena in certain II–VI nanocrystal systems.[23]

Linear $\mathbf{k}^*\mathbf{p}$ theories provide the starting point for this discussion. The one electron wave function of the solid is in the form $\psi_{\mathbf{k}}=u_{\mathbf{k}}(\mathbf{r})e^{i\mathbf{k}\cdot\mathbf{r}}$. Here, $u_{\mathbf{k}}$ is a linear combination of atomic orbitals which describe a single state within a unit cell. The amplitude of this state from unit cell to unit cell is described by the exponential (Bloch) term. To extend this description to finite size, it is useful to first transform these wave functions to a spherical coordinate system, and to then find the eigenvalues of the resulting (spherical) Hamiltonian in the presence of the confinement and/or Coulomb potential. A commonly used approximation is to ignore the cubic nature of the lattice, and assume a spherical unit cell.[24] This transformation yields a single conduction band, and a valence band that is split into two branches, the light and heavy holes. In an analogous manner to the vibrations, the heavy hole states correspond to p-orbitals which are transverse to the radial wave vector, and thus have π-type bonding interactions along the radial direction (Fig. 2, Col. II, top left). The light hole branch corresponds to p-orbitals which are longitudinal with respect to the radial wave vector and thus have σ-type bonding interactions in the radial direction (Fig. 2, Col. II, top right). These orbitals can be written in terms of the usual x, y, z p-orbital basis sets. For example, the heavy hole states oriented along z and light hole states oriented along the x direction are given as follows:

$$
\begin{aligned}
|HH(k)\rangle_z=&\frac{1}{\sqrt{2}}\left(j_0(kr)Y_0^0+\sqrt{\frac{2}{5}}\,j_2(kr)Y_2^0\right)|p_z\rangle\\
&-\sqrt{\frac{3}{10}}\,j_2(kr)\,\frac{(Y_2^1+Y_2^{-1})}{\sqrt{2}}\,|p_x\rangle,\\
|LH(k)\rangle_x=&\frac{1}{\sqrt{2}}\Bigg(j_0(kr)Y_0^0+\Bigg(\sqrt{\frac{1}{10}}\,Y_2^0\\
&+\sqrt{\frac{3}{5}}\,\frac{(Y_2^2+Y_2^{-2})}{\sqrt{2}}\Bigg)j_2(kr)\Bigg)|p_x\rangle\\
&-\sqrt{\frac{3}{20}}\,j_2(kr)\,\frac{(Y_2^1+Y_2^{-1})}{\sqrt{2}}\,|p_z\rangle.
\end{aligned}
\tag{8}
$$

$|p_{z,x}\rangle$ are the individual atomic basis functions oriented along z or x. The angular dependence, introduced through the spherical harmonics Y_m^n simply reflect the fact that an orbital which is tangential to the sphere at the equator is radially directed at one of the poles. This is illustrated in the top of Fig. 2, Col. II. The *general* equation for a hole state is thus:

$$
\begin{aligned}
\phi_{h,F_z}(r)=&A\Bigg[j_0(kr)Y_0^0+j_2(kr)\\
&\times\sum_{m+\mu=F_z}\langle 1,\mu,2,m|1,F_z\rangle Y_2^m\Bigg]|p_\mu\rangle.
\end{aligned}
\tag{9}
$$

The coefficients $\langle L1,m1_z,L2,m2_z,|F,F_z\rangle$ in the hole wave function are the Clebsch–Gordan coefficients addition of angular momentum states $L1$ and $L2$ to form a state with total angular momentum F. The distinction between the light and

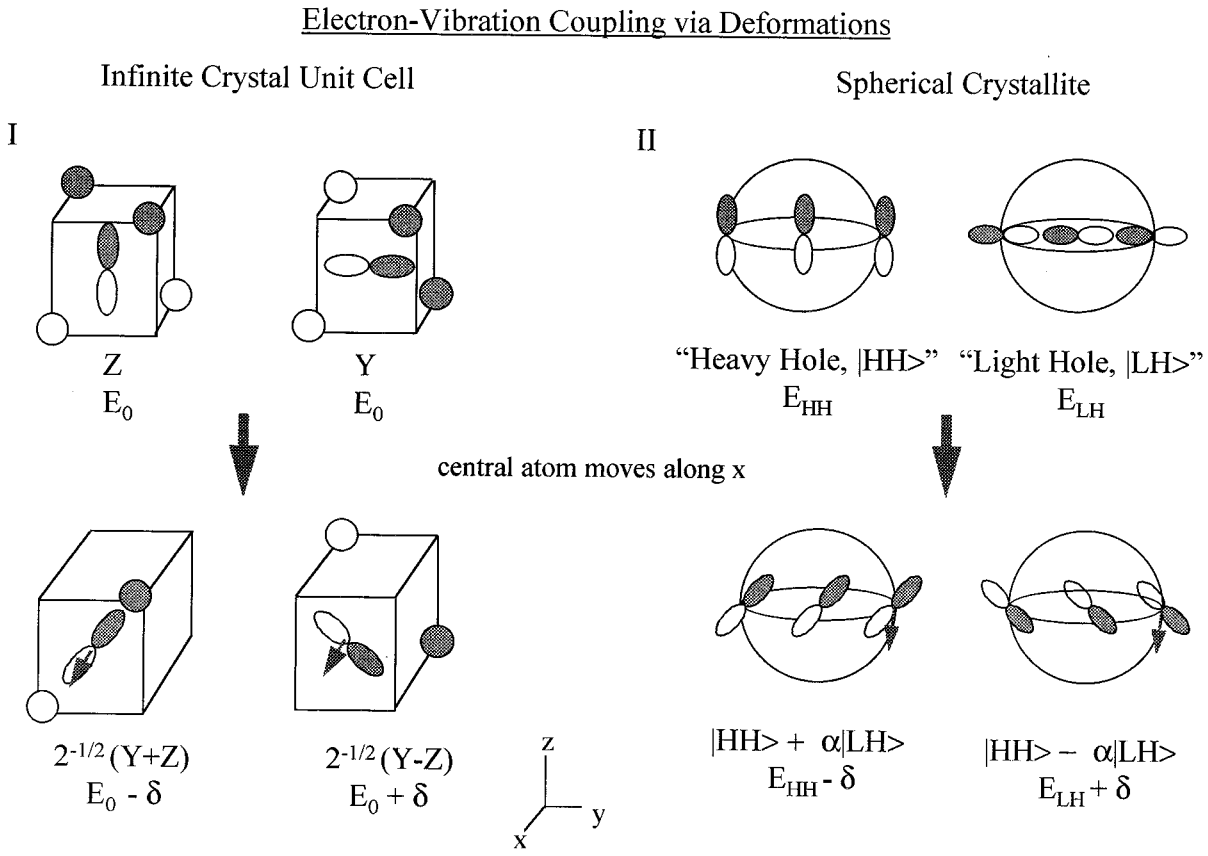

FIG. 2. The mechanism of optical mode deformation potential coupling in infinite and finite systems. Column I illustrates the orbital rehybridization upon excitation of an optical mode in an infinite crystal. At the top are the orbitals corresponding to the undistorted tetrahedron. At the bottom are the new orbitals resulting from motion of the central atom. In Column II, the light hole and heavy hole orbitals (top) of a sphere are mixed by a transverse optical phonon.

heavy holes is reflected in $F_z:0$ corresponding to σ-type bonding, ± 1 to π-bonding. A is the normalization constant. Our discussion so far has neglected the effects of spin-orbit coupling. In general, the effects of spit-orbit coupling on the deformation potential are quite small. This is not surprising, given that the above argument depends upon the spatial parts of the orbitals being rotated into each other.

The spherical Hamiltonian, and the resulting heavy and light hole orbitals, are a starting point for the calculation of the electronic states in a finite nanocrystal. A final approximation is to neglect the Coulomb coupling between charge carriers, allowing only the confinement potential to act on the charge carriers.[20,21] The confinement potential requires that the envelope function goes to zero at the boundary of the particle. This causes the heavy and light hole states to mix, leading to the following equation for the allowed states κ:

$$j_0(\kappa)j_2(\beta^{1/2}\kappa)+j_0(\kappa)j_0(\beta^{1/2}\kappa)=0, \tag{10}$$

where $\beta=m_H/m_L$, which is the ratio of the bulk light and heavy hole masses. The light and heavy hole masses are thus only material dependent parameters needed to describe the hole states within this model. These masses may be calculated from the Luttinger parameters given in Table I.[24] In the spherical approximation, $m_H=(\gamma 1+2(0.4\gamma 2+0.6\gamma 3))^{-1}$ and $m_L=(\gamma 1-2(0.4\gamma 2+0.6\gamma 3))^{-1}$. The hole energies are then:

$$E=\frac{(\hbar\kappa)^2}{2m_H R^2}, \tag{11}$$

and the wave functions (following the notation of Efros[20]), indexed by κ are given by:

TABLE I. The physical parameters used to model the InP LO/TO ratio. $\gamma 1-3$ are the experimental Luttinger parameters from Ref 38. d_0, the optical deformation potential, is taken from Ref. 9. The remaining parameters were taken from Ref 49. *me* is the mass of the electron (in units of electron mass). $\hbar\omega_{\mathrm{TO/LO}}$ are the LO and TO frequencies in cm^{-1}. ν_s is the sound velocity. ϵ_∞ and ϵ_0 are the optical and static dielectric constants, a is the zinc-blende lattice parameter. (D_e-D_h) is the band gap deformation potential, and C_{11} is an elastic constant. E_g is the band gap.

$\gamma 1$	$\gamma 2$	$\gamma 3$	*me*	$\hbar\omega_{\mathrm{TO}}\ \mathrm{cm}^{-1}$	$\hbar\omega_{\mathrm{LO}}\ \mathrm{cm}^{-1}$	ν_s (Å/ps)
4.95	1.65	2.35	0.08	308	348	51.3
ϵ_∞	ϵ_0	a(Å)	d_0(eV)	(D_e-D_h)(eV)	C_{11} erg cm^3	E_g(eV)
9.6	12.61	5.87	31.2	6.35	10.22	1.41

$$\phi_\kappa = \left[HH(\kappa/R)\rangle - \left(\frac{j_0(\kappa)}{j_0(\kappa\beta^{1/2})} \right) \middle| LH(\kappa\beta^{1/2}/R)\rangle \right], \quad (12)$$

where the normalization factor is

$$\frac{1}{A^2} = \int_0^1 \Pi_0^2(r) + \Pi_2^2(r) r^2 \, dr. \quad (13)$$

Π_0 and Π_2 are given by

$$\Pi_0(r) = \left(j_0\left(\frac{\kappa r}{R}\right) - \frac{j_0(\kappa)}{j_0(\kappa\beta^{1/2})} j_0\left(\frac{\kappa\beta^{1/2} r}{R}\right) \right),$$
$$\Pi_2(r) = \left(j_2\left(\frac{\kappa r}{R}\right) + \frac{j_0(\kappa)}{j_0(\kappa\beta^{1/2})} j_2\left(\frac{\kappa\beta^{1/2} r}{R}\right) \right). \quad (14)$$

The lowest confined conduction band states are then given by the standard expression

$$\phi_e(r) = B j_0\left(\frac{\pi r}{R}\right) Y_0^0 |s\rangle,$$
$$B = \left(\frac{1}{R^3 (\int_0^1 (j_0(\pi r))^2 r^2 \, dr)} \right)^{1/2}, \quad (15)$$

with energies given by

$$E = \frac{(\hbar \pi)^2}{2 m_e(R) R^2} \quad (16)$$

with m_e as the electron mass. Since the conduction band is nonparabolic in InP, we vary the effective mass as a function of R to match the conduction band dispersion calculated using a tight-binding model.[25] The confinement energy is the sum of its electron and hole components. In Fig. 3, the experimental and model band gaps are plotted (solid line). Clearly, while the general physical trend is reproduced in the theoretical curve, the theory greatly overestimates (by about 50%) the effects of confinement. Thus we also present a plot of the model band gap vs $1.25*R$. This same normalization will be referred to later in Sec. VI when Raman cross-section ratios are presented. Both curves were calculated using the parameters in Table I.

These are the wave functions that we shall use to describe the electron, light hole, and heavy hole states in the subsequent resonance Raman cross-section calculation. These wave functions also permit the calculation of the transition dipole moment, μ_κ, for any given transition through the use of

$$\mu_\kappa = \frac{\langle s|X|p_x\rangle}{AB} \int \Pi_0^\kappa(r) \phi_e(r) r^2 \, dr. \quad (17)$$

The wave functions are generic for any semiconductor that have near-parabolic conduction and valence band edges near $k=0$.

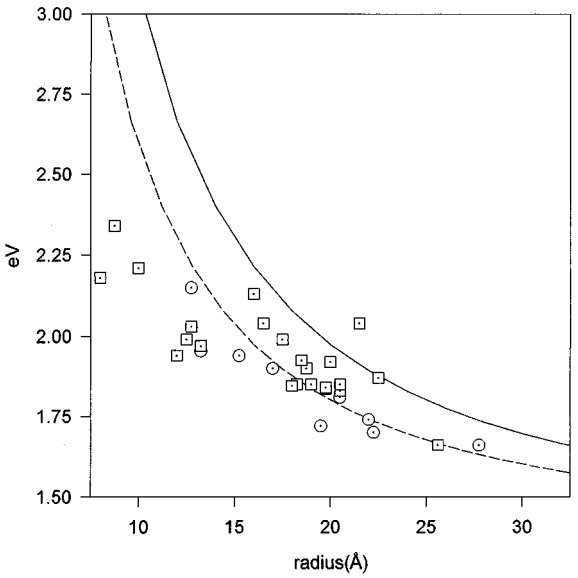

FIG. 3. Comparison of model and calculated confinement energies for the lowest state. The experimental points are from Ref. 7; the solid line are the results from using the model energy level calculations. The dotted line is the result of scaling the radius by a factor of 1.25 to give better agreement with the data.

IV. RESONANCE RAMAN THEORY

In the previous sections we have discussed how the electronic and vibrational states are changed by the imposition of finite size, and we have demonstrated that all three types of optical modes are in principal Raman active. Now we will begin to address the question of how the Raman intensities are modulated by finite size. In the following paragraphs we introduce the standard equations for Raman scattering in molecular systems. These equations require three inputs: the Franck–Condon overlaps between the ground and excited states; the dipole moment derivatives; and the excited state lifetime. In subsequent sections, we will show how to calculate the first two of these inputs for the case of a finite, spherical nanocrystal. The calculation of the size dependent acoustic phonon contribution to the excited state lifetime is described in several references.[26,27] In the case of InP, a recent study has shown that this mechanism is the dominant one in InP, due to the covalent nature of the lattice, which leads to a large acoustic mode deformation potential.[28]

In finite size, the electronic states become discrete and relatively well separated. This means that one can take advantage of the formulations commonly used in molecular spectroscopy to describe optical processes. For Raman scattering, a convenient starting point is based on Albrecht's formalism for calculating the elements of the Raman amplitude tensor, $\alpha_{\rho\sigma}$, where the laser, ν_0, is in resonance with a single excited state, e:[29]

$$\alpha_{\rho\sigma}=\sum_n \frac{\langle gf|\mu_e^{\rho}(q)|en\rangle\langle en|\mu_e^{\sigma}(q)|gi\rangle+\langle gi|\mu_e^{\rho}(q)|en\rangle\langle en|\mu_e^{\sigma}(q)|gf\rangle}{\nu_{en}-\nu_0+i\gamma_e}. \tag{18}$$

μ^{σ} is the transition dipole moment along the direction σ, ν_{en} denotes the energies of each vibronic intermediate state en and γ_e is the excited state lifetime. The states are labeled according to Albrecht, gi is the initial vibrational state in the ground electronic surface, en is the nth vibrational of the state in the excited state, gf is the final state on the ground electronic surface. Taylor expanding $\mu(q)$ and using perturbation theory to find the first derivative μ':

$$\begin{aligned}\mu_e(q)&=\mu_e+\mu_e^{'}q+O(q^2),\\ \mu_e^{'}&=\sum_s \frac{h_{es}^{q}\mu_s}{\nu_s-\nu_e}.\end{aligned} \tag{19}$$

The subscript s denotes higher excited states, $h^q{}_{es}$ is the vibration induced coupling between the two excited states. In our systems such coupling is caused by the deformation potential.[30] We now divide the expression for the Raman amplitude into two terms, A and B:

$$\begin{aligned}A_{\sigma\rho}&=\frac{1}{\hbar}\sum_n \frac{\mu_e^{\rho}\mu_e^{\sigma}\langle gf|en\rangle\langle en|gi\rangle}{\nu_{en}-\nu_0+i\gamma_e},\\ B_{\sigma\rho}&=-\frac{1}{\hbar^2}\sum_{s,n} h_{es}^{a}\frac{\mu_e^{\rho}\mu_s^{\sigma}\langle gf|en\rangle\langle en|q_a|gi\rangle+\mu_e^{\sigma}\mu_s^{\rho}\langle gi|en\rangle\langle en|q_a|gf\rangle}{(\nu_s-\nu_e)(\nu_{en}-\nu_0+i\gamma_e)}.\end{aligned} \tag{20}$$

The A term, or constant dipole moment term, is only active on or near resonance for modes which have A_1 symmetry. The intensity of these modes depends on the magnitude of the Franck–Condon factors $\langle gf|en\rangle$. If the vibrational mode is harmonic and has the same frequency in both the excited and ground state, these overlap terms are functions of a single parameter, Δ.[31] Δ describes the shift in the position of the vibrational minimum between the ground and excited state surfaces. A shift in the minimum means that at the instant of optical excitation there is potential energy stored in the lattice. The amount of potential energy is given by

$$PE=\tfrac{1}{2}\,m\omega^2\Delta^2, \tag{21}$$

and the corresponding number of virtual phonons is $S=\Delta^2/2$.

The B term, which results from variation in the dipole moment as a function of nuclear coordinate, is responsible for off-resonance scattering and scattering by modes which are not A_1. Upon optical excitation, the center of the nuclear wave function is initially shifted from the ground state equilibrium position by an amount proportional to μ'. The total Raman cross section is given by $|\alpha|^2$; A terms scale as the potential energy deposited into the lattice upon optical excitation and the B terms scale as $(|\mu'|)^2/2$.

In understanding the distinction between the A and B terms, it is helpful to recast the Albrect formalism into the time-dependent formalism of Heller *et al.*[31,32] This is illustrated in Fig. 4. Column I describes the A term; the wave function describing the excited state nuclear positions is initially centered at the ground state equilibrium position and oscillates in time. The resulting overlap, $\langle 1|0(t)\rangle$ shown in the bottom of Fig. 4, Col. I, is the time evolution of the Raman amplitude, and it is *initially zero*. Column II illustrates the B term. Along this coordinate, the ground and excited state potential energy surfaces are aligned, but the wave function describing the excited state nuclear positions is not centered at the equilibrium position, and thus oscillates in time. The resulting overlap, $\langle 1|0(t)\rangle$ (Fig. 4, Col. II, bottom), is initially at its maximum. The excited state dephasing rate, $\Phi(t)$ (Fig. 4, Col. III, top), serves to window the Raman overlap $\langle 1|0(t)\rangle$. The function $\Phi(t)=\exp(-\gamma_e t)$ corresponds to the decay rate implied in Eq. (20). Within the context of the time-dependent picture, we are able to choose other forms for the excited state dephasing, such as those corresponding to a bath of low frequency oscillators.[33] The final excitation profile, as a function of laser frequency ω, is shown in the bottom of Fig. 4, Col. III. It is obtained through Fourier transfomation of the product $\langle 1|0(t)\rangle\Phi(t)$, and thus the Raman amplitude and cross section depend on the rate of the excited state dephasing.

The fact that the nuclear wave packets are launched at different points on the excited state surface means that the two terms are effected by the excited state lifetime in different ways. For A term scattering the Raman intensity is strongly modulated by the excited state lifetime: the longer the lifetime, the greater the Raman intensity. The A term becomes very small in the limit of short lifetimes. B term scattering, in which the intensity is developed instantaneously, does not go to zero in the limit of short lifetimes. Thus short lifetimes enhance the B term scattering relative to A term. For sufficiently long lifetimes, both the B term and A term intensity are affected equally.

V. DEFORMATION POTENTIAL COUPLING OF ELECTRONIC STATES IN FINITE SIZE

In this section we calculate the expected Raman cross sections considering only local deformation potential cou-

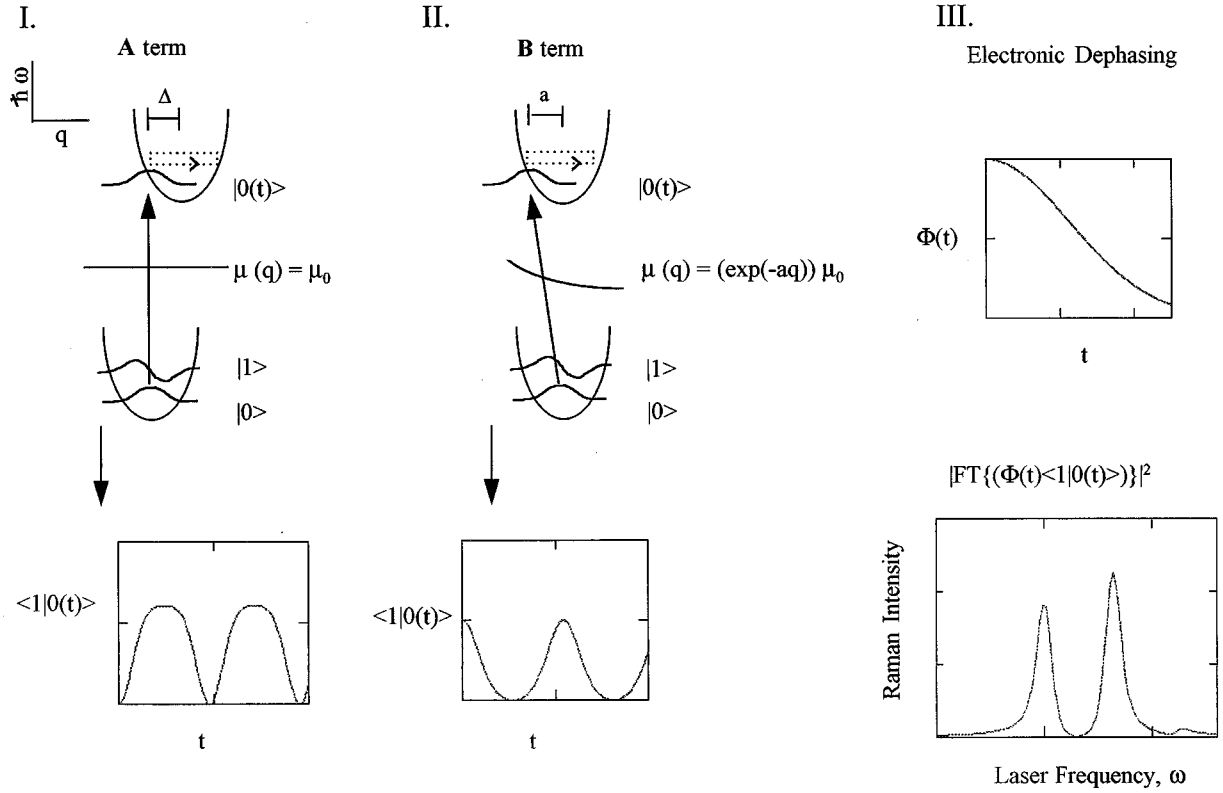

FIG. 4. Time-dependent pictures of Raman scattering. Column I illustrates the case (*A* term) where the transition dipole moment μ, is independent of nuclear coordinate. The bottom of Column I shows the time-dependent overlap of the excited wave packet state with the first excited vibrational level in the ground electronic state. Column II illustrates the nonconstant dipole case (*B* term). The top of Column III shows a typical dephasing rate that results from the classical oscillator model discussed in the text [Eq. (46)]. The bottom of Column III shows the Raman excitation profile that results from the convolution of the overlap integral $\langle 1/0(t)\rangle$ with the excited state dephasing rate, given by $\Phi(t)$.

pling. Long-range coupling (important for the LO mode) is considered later. For short-range coupling, we need two inputs to calculate the nanocrystal size-dependent Raman cross sections. The first input is the quantity h_{es} in the Albrecht *B* term of Eq. (18). Physically, this corresponds to the energy shift, δ, in the bottom of Fig. 2 and it is directly related to the optical deformation potential. The second input is the energy level spectrum, which we obtain using the spherical k^*p model. These inputs yield the polarizability density; i.e., the contribution that each unit cell makes to the Raman amplitude. We need to integrate this density over the entire crystallite. The integral is weighted by the convolution of the envelope function of the vibrational modes (Sec. II) with the envelope functions of the electronic states (Sec. III).

The procedure is illustrated in Fig. 2. The undistorted unit cell has T_d symmetry (Fig. 2, Col. I, top) and the x, y, and z molecular orbitals between a central p-orbital and the peripheral s-orbitals are degenerate. When the central atom moves along the x axis, the new unit cell symmetry becomes C_{2v}, the x, y, z degeneracy of the orbitals is lifted, and all orbitals now have different symmetry labels. This is indicated in the bottom of the Fig. (Fig. 2, Col. II, bottom). The x-orbital, to first order, remains constant in energy, but the y and z orbitals are split and rotated. We now wish to connect the individual unit cell model (Fig. 2, Col. I) to the case of a spherical crystallite. (Fig. 2, Col. II). In this case the highest occupied orbitals are those which involve linear combinations of the p-orbitals parallel to the surface (''heavy holes''). Orbitals that point inward, the light holes, are more tightly bound than the tangential, heavy hole, orbitals. Upon excitation of a TO mode (motion tangential to the surface of the sphere) these two orbitals are rotated into each other (Col. II, bottom). Simple perturbation theory arguments suggest that the magnitude of this effect varies linearly in the magnitude of the displacement; i.e., $1/R^{3/2}$, [Eq. (5)], and the energy difference between the two confined states $(1/R^2)$. *Thus the Raman amplitude should scale as* $R^{1/2}$ *and the intensity should scale linearly in R.* Upon excitation of an LO mode, the two heavy hole orbitals are rotated into each other, but in opposite directions on opposite sides of the sphere resulting in no net effect. Thus deformation potential coupling is not operative for LO modes. This is totally consistent with the selection rules that have been observed in MBE deposited layers of GaAs.[34]

In the bulk, at $k=0$, excitation of an optical phonon causes the otherwise degenerate light and heavy hole states to split by an amout $d\epsilon$. This energy splitting is given by[9,30]

$$d\epsilon = d_0 \delta_{\text{bond}}, \tag{22}$$

where δ_{bond} is the fractional change in the bond length. According to degenerate perturbation theory, the vibration in-

duced splitting at any point in k-space is calculated using the following Hamiltonian, written in the basis of the unperturbed heavy and light hole states:

$$H = h_0(k) + h_{ev} = \begin{pmatrix} E_{\mathrm{HH}}(\mathbf{k}) & d_0\delta_{\mathrm{bond}} \\ d_0\delta_{\mathrm{bond}} & E_{\mathrm{LH}}(\mathbf{k}) \end{pmatrix}. \tag{23}$$

To extend this result to finite size, we use Eq. (12) to write each confined wave function in terms of its light and heavy hole components. The *confined* Hamiltonian between any two states, ϕ_κ and φ_0, is now given by

$$H = h_0(R) + h_{ev}^a, \tag{24a}$$

$$h_0 = \begin{pmatrix} E_0(R) & \\ & E_\kappa(R) \end{pmatrix}, \tag{24b}$$

$$h_{ev}^a = \begin{pmatrix} 0 & d_0\langle\varphi_0|\chi^a(\mathbf{r})|\phi_\kappa\rangle \\ d_0\langle\phi_\kappa|\chi^a(\mathbf{r})|\varphi_0\rangle & 0 \end{pmatrix}, \tag{24c}$$

where $\chi^a(r)$ is the envelope function of the vibration. The matrix element is given by the following integral:

$$\langle\varphi_\kappa|\chi^a(r)|\phi_0\rangle = \frac{\int_0^1(\Lambda_{\kappa 0}+\Lambda_{0\kappa})r^2\,dr}{A_\kappa A_0}\left(\frac{\hbar a^3}{4M\omega I_{20}R^3}\right)^{1/2},$$
$$\Lambda_{\mu\nu} = \int \sum_m \varphi_2(\zeta_\alpha r) Y_2^m \langle HH|\varphi_0\rangle\langle LH|\phi_\kappa\rangle\,\delta\Omega, \tag{25}$$

where Π_0, Π_2, and A are defined in Sec. III; the factor in parenthesis following the integral is the phonon normalization factor for the lowest Raman active TO mode (see Sec. II) which scales the magnitude of the displacement. Terms such as $\langle HH|\varphi_\kappa\rangle$ are evaluated using Eqs. (9), (10), and (12).

The calculation proceeds in three basic steps. First, we find the unperturbed electron levels and relative contributions of the electron and hole using the spherical **k***p theory to form $h_0(R)$ [Eq. (24b)]. We use the **k***p wave functions, and the TO vibration envelope functions [Eq. (7)] to form h_{ev} in Eqs. (23c) and (24). We then find eigenvectors of the vibrationally perturbed Hamiltonian, $|\nu\rangle = a_\nu|\varphi_\kappa\rangle + b_\nu|\phi_0\rangle$.

We now compute the magnitude of the Albrecht B term using Eq. (20). The term $h_{es}/(\Delta\nu_{es})$, valid for nondegenerate perturbation theory, is replaced by the ratio $a_\nu b_\nu$ (for $a_\nu > b_\nu$) to yield the amount of higher excited state that displacement along TO mode coordinate introduces into the initial hole state. Finally, we compute the transition dipole moment, μ_κ, for each state κ [Eq. (17)] and perform the summation (including the six lowest states). The final result for the fractional change in the transition dipole moment is:

$$\frac{d\mu_0}{\mu_0} = \left(\sum_i \frac{a_\nu}{b_\nu}\frac{\mu_i}{\mu_0}\right). \tag{26}$$

The total cross section scales as $(|\mu'|)^2/2$. In order to compare this result to the LO mode scattering intensity, it is important to consider the details of the scattering geometry. The LO modes have A_1 symmetry and all light scattering is polarized. The TO modes are not A_1 and thus will have depolarized scattering. Equation (22) yields the Raman tensor element α_{xy}. Using this we can compute the total intensity scattered into the y direction under x polarized excitation. This is 3/4 of the scattering along the x direction. Thus the cross section derived from Eq. (26) should be multiplied by 8/3 to give the *total* scattering intensity both parallel and perpendicular to the excitation. The adjusted cross section is plotted as a function of R in Fig. 5 (top). As expected for small R, this function is linear.

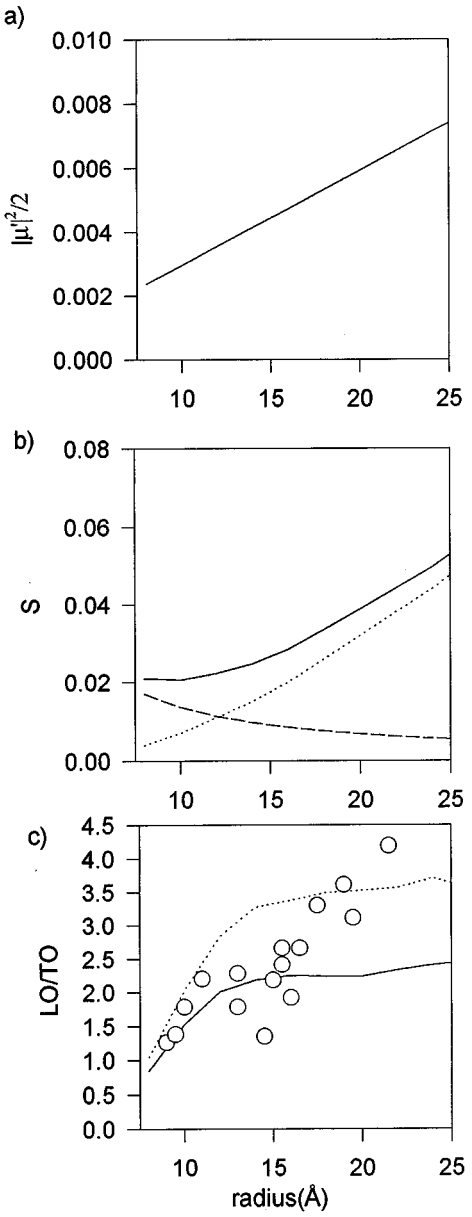

FIG. 5. Calculated phonon couplings vs size. The top panel is a plot of the square of the transition dipole moment, $|\mu'_{\mathrm{TO}}|^2/2$ as a function of nanocrystal radius. This scales size dependence of the TO mode Raman intensity. The middle panel shows the calculated results of the two components of S_{LO} versus radius. The dotted line are the results of the analytic term given by Eq. (31). The dashed line are the result of the polaron model calculation. The sum scales the LO mode intensity. The bottom panel is a comparison of the experimental results (Ref. 42) (open circles) and the results of a Raman cross section calculation (solid line) using the calculated values for S and $|\mu'_{\mathrm{TO}}|^2/2$ given in the top two panels and the dephasing rate from Eq. (46).

VI. COUPLING TO LO MODES (FRÖLICH)

Having computed the short-range effects, we now turn to very different problem of coupling to the polar modes of the lattice. Recall that in Sec. I we discussed that when a charge carrier is placed into a dielectric, energy is stored in the dielectric in the form of nuclear displacement. For a single charge carrier we can compute the number of accompanying virtual phonons [which is equivalent to $S(=\Delta^2/2)$ in the Raman formalism] by using the following second order perturbation series expansion (valid for low temperatures):[35]

$$\hbar\omega S=\frac{|\langle k,1_0|h_{l0}|k,0_0\rangle|^2}{\hbar\omega}+\sum_{q>0}\ \frac{|\langle k,1_q|h_{l0}|k,0_q\rangle|^2}{\epsilon_{k+q}-\epsilon_k+\hbar\omega}, \tag{27}$$

where h_{l0} is given by

$$h_{l0}=\frac{-i}{q}\left[\frac{\hbar\omega e^2}{V}\left(\frac{1}{\epsilon_\infty}-\frac{1}{\epsilon_0}\right)\right]^{1/2}(a_n+a_n^+). \tag{28}$$

V is the volume of the crystal, k refers to the electronic state wave vector, $0_q(1_q)$ the population state of a phonon of wave vector q. Due to the form of h_{l0}, there are no first order energy terms. The first term on the right side of Eq. (27) represents the energy shift with no change of electronic state, and the second term is the energy shift induced by coupling to higher electronic states. In the presence of two oppositely charged carriers, this series expansion is much more difficult to carry out, as one must consider both bound exciton and unbound plane wave states.

For a static, bound charge distribution, the first term in the perturbation series is readily evaluated and is given by

$$P(r)=e(\varphi_h^2(r)-\varphi_e^2(r)), \tag{29}$$

where $P(r)$ is the excited state charge distribution. Using the spherical $\mathbf{k}^*\mathbf{p}$ wave functions and the forms for the confined vibrational wave functions presented in Sec. II, h_{l0} is now given by[36]

$$h_{lo}=\left[\frac{\hbar\omega e^2}{R}\left(\frac{1}{\epsilon_\infty}-\frac{1}{\epsilon_0}\right)\right]^{1/2}(a_n+a_n^+), \tag{30}$$

and the following analytical results is obtained for its contribution to S:

$$S_n^0=\left[\frac{\hbar\omega e^2}{2RI_{1n}}\left(\frac{1}{\epsilon_\infty}-\frac{1}{\epsilon_0}\right)\right]\left(\int_0^1\left(\frac{\Pi_2^2(r)+\Pi_0^2(r)}{A^2}-\varphi_e^2(r)\right)j_0(\nu_n r)r^2\,dr\right)^2. \tag{31}$$

The most salient feature is that S^0 goes as $1/R$ and thus goes to 0 in the bulk. The results of Eq. (31) are plotted in dashed line of the middle plot of Fig. 5. The dependence on R results from the fact that as the volume expands, the density of charge decreases. Inclusion of Coulomb coupling changes the results slightly. The most noticeable effect is a small increase of the coupling in extremely large (>150 Å) sizes away from the dominant $1/R$ trend.[15] In the bulk, however, many experiments have indicated that there is substantial polar coupling.[37] Furthermore, there are several resonance Raman experiments which have demonstrated that the overall trend is toward increased coupling as the radius is increased.[2,38] Indeed, this is what one might expect from examination of the *single* charge carrier expression in Eq. (27). There the presence of an energy denominator in the second term suggests that the S will decrease in magnitude with decreased radius. Thus we expect that the number of virtual phonons (S) (and thus the LO scattering intensity) for a very small crystallite will exhibit a $1/R$ dependence, but that S will increase with size for intermediate sized crystallites. This is in qualitative agreement with the InP experimental results (Fig. 5, bottom). Thus it is necessary to develop some scheme for estimating the magnitude of this second term. While a direct calculation using perturbation theory is conceptually simple, it suffers from the fact that there are a large number of terms which need to be considered and convergence is slow for larger crystallites. This is what will motivate our appeal to the solutions of the coupled polaron problem in the bulk, which is a variational approach to solving the problems posed by h_{l0}. What the remainder of this section does is to present one such solution, valid for coupled charge carriers in a bulk lattice, and then examine the effects of confining the charge carriers to an ever decreasing volume.

The coupled polaron problem has a long history. Briefly, one wants to develop an effective potential for the interaction of two charge carries that are screened from each other by a polar lattice. In the bulk this leads to the following Hamiltonian:[13]

$$H=\frac{P^2}{2M}+\frac{p^2}{2\mu}-\frac{e^2}{\epsilon_\infty r}+\sum_k\ \hbar\omega a_k^+a_k+\sum_k\ \frac{V}{k}\,\rho(k,r)e^{ik\cdot R}+\text{H.c.} \tag{32}$$

with the following definitions:

$$\rho(k,r)=e^{is_h\mathbf{k}\cdot\mathbf{r}}+e^{-is_e\mathbf{k}\cdot\mathbf{r}},$$
$$V=-i\left(\frac{2\pi e^2\hbar\omega}{\nu\epsilon^*}\right)^{1/2},$$
$$S_{e,h}=\frac{m_{e,h}}{M};\quad M=m_e+m_h;\quad \mu=\frac{m_em_h}{M}, \tag{33}$$
$$\frac{1}{\epsilon^*}=\frac{1}{\epsilon_\infty}-\frac{1}{\epsilon_0}.$$

This Hamiltonian is similar in form to the single polaron case treated by Lee, Low, and Pines.[11] The major differences are the inclusion of a Coulomb attraction, and the fact that the interaction with the lattice now depends on two particles, not one. One approach to this problem was originally outlined by Haken[39] and refined by Pollman and Buttner.[13] They assume that the total wave function has the form $U_1U_2|0\rangle\phi(r,R)$, where $|0\rangle$ is the phonon ground state, $\phi(r,R)$ the electronic wave function. The coordinate transformations U_1, U_2 are given by

$$U_1=\exp\left[i\left(Q-\sum_k \mathbf{k}a_k^+ a_k\right)\cdot R\right],$$
$$U_2=\exp\left[\sum_k F^*(k,r)a_k+F(k,r)a_k^+\right]. \tag{34}$$

Q is the total momentum of the system, the two charge carriers, and the momentum of the phonons. U_1 eliminates the center of mass coordinate from the coupling to the lattice, leaving us only with the problem of solving the relative motion of two charge carriers in a dielectric medium. U_2 represents a shift of the phonon coordinates in the presence of the electron and the hole to a new minimum. U_2 operating on the ground state wave function, $|0\rangle$, is exactly analogous to the shift in phonon coordinate implicit in the Albrecht A term type scattering. We can reinforce this point by noting the similarity between the role that the $F(k,r)$ play and the description of an excited state Hamiltonian as a shifted oscillator:

$$H_{\rm ex}=\left[e^{(\Delta a-\Delta a^+)}\right]H_g. \tag{35}$$

The problem then becomes one of choosing a suitable form for $F(k,r)$. Pollman and Buttner tried a number of different forms; the one that they found most useful is

$$F(k,r)=\frac{V}{\hbar\omega}\,(f_e(k)e^{is_h\mathbf{k}\cdot\mathbf{r}}-f_h(k)e^{is_e\mathbf{k}\cdot\mathbf{r}}), \tag{36}$$

where the $f_{e,h}(k)$ are the displacement amplitudes for the electron and the hole. This ansatz has proved useful in describing the behavior of excitons not only in weakly bound, mostly covalent systems such as GaAs, where the exciton is large, but also in highly polar, tightly bound systems such as CuCl. The $f_{e,h}(k)$'s are chosen via a variational minimization procedure which results in the following form:

$$f_{e,h}=\frac{(1-G)(1+R_{h,e}^2k^2+G)}{(1+R_h^2)(1+R_e^2)-G^2}, \tag{37}$$

where $R_{h,e}$ are the polaron radii of the hole and the electron, and

$$G(k)=\langle\phi_e\phi_h|e^{i\mathbf{k}\cdot\mathbf{r}}|\phi_e\phi_h\rangle,$$
$$=\langle\phi_e|e^{i\mathbf{k}\cdot\mathbf{r}_e}|\phi_e\rangle\langle\phi_h|e^{-i\mathbf{k}\cdot\mathbf{r}_h}|\phi_h\rangle. \tag{38}$$

The second line is valid in the limit where the Coulomb energies are weak relative to the confinement energy, allowing the use of the product wave functions derived from the $\mathbf{k}^*\mathbf{p}$ treatments and explicit substitution $\mathbf{r}_e-\mathbf{r}_h$ for $\mathbf{r}$. The f's depend implicitly on the size of the wave function through $G(k)$. In the limit of very extended wave functions, the independent polaron limit of $1/(1+R_{e,h}^2)$ is recovered. For small wave functions, the values of $f(k)$ are greatly suppressed from this value. Even when the charge carriers are well separated, there is still suppression. For example, wave functions which have an average separation of the two charge carriers of 2–3 times the combined polaron radii still have a 10%–20% reduction in the coupling to the lattice.

Our knowledge of the forms of $\phi_{e,h}$ suggest the following expansion for $e^{i\mathbf{kr}}$:

$$e^{-i\mathbf{k}\cdot\mathbf{r}_{e,h}}=4\pi\sum_l\sum_{-l\leqslant m\leqslant l}(-i)^l j_l(kr_{e,h})Y_{l,-m}(\Omega_{e,h})$$
$$\times Y_{l,m}(\Omega_k). \tag{39}$$

The terms in Y_{00} lead to LO mode scattering, whereas the terms in higher order lead to mixed or surface mode scattering. Direct substitution leads to the following equation for $G(k)$:

$$G(k)=\frac{1}{A^2}\int_0^1 j_0(kr_h)\left(\Pi_0^2(kr_h)+(\Pi_2^2(\kappa r_h))r_h^2\,dr_h\right.$$
$$\times\int_0^1 j_0(kr_e)\varphi_0^2(\pi r_e)r_e^2\,dr_e, \tag{40}$$

where A, Π_0, Π_2, φ_e, are all defined in Sec. III. The total energy deposited into the each vibrational mode, k, is

$$D(k)^2=\langle\phi_e\phi_h||F_k(r)|^2|\phi_e\phi_h\rangle, \tag{41}$$

which can be computed by squaring Eq. (35) and evaluating the integral over the electron and hole coordinates

$$D^2(k)=f_e^2(k)+f_h^2(k)-2f_e(k)f_h(k)G(k). \tag{42}$$

The sum

$$S_{\rm LO}=\sum_k D_k^2\rightarrow\int_0^{k\ \max}D(k)_k^2k^2\,dk \tag{43}$$

gives the total number of LO phonons generated by the second term in Eq. (27). To find the total of both terms we add the results of Eq. (43) to Eq. (30). In the absence of significant lifetime effects, this is proportional to the resonance Raman intensity. The evaluation of this equation as a function of R is shown in Fig. 5 (middle, dotted line). The addition of Eq. (31) and Eq. (43) is shown as the solid line of the middle plot of Fig. 5. Thus we are able to calculate $S_{\rm LO}$, $\mu'_{\rm TO}$.

The final input, the excited state dephasing rate, $\Phi(t)$, is calculated assuming that the dominant contribution to the line width are low frequency acoustic vibrations. see Refs. 29 and 38. These vibrations act like a third coupled vibrational mode which has shift, Δ_{ac} given by[40]

$$\Delta_{ac}=\frac{0.97^2(D_e-D_h)^2}{\pi R^3C_{11}\hbar\omega_{ac}}, \tag{44}$$

where the frequency of the confined acoustic modes is given by

$$\omega_{ac}=\frac{\zeta_{ac}}{R}\,\nu_s. \tag{45}$$

C_{11} is the 11 elastic constant, (D_e-D_h) is the acoustic mode deformation potential, v_s is the sound velocity, and ζ_{ac} is the appropriate root which makes the acoustic mode wave function vanish at the crystallite boundary.[26] [For the lowest lon-

gitudinal acoustic modes these are the roots of $j_1(x/R)$.] This leads to the following equation for the dephasing rate in the classical, high temperature limit:[33]

$$\Phi(t)=\exp\left(\omega\,\frac{\Delta^2}{2}\left(it-\frac{k_bTt^2}{\hbar}\right)\right). \tag{46}$$

Although for some of the frequencies and temperatures involved, the use of the classical limit might seem unwarranted, the experimental time-dependent photon echo data[28,38] demonstrates none of the recurrences which are present in the nonclassical case. We simulate the effects of the crystallite size distribution by using a broad inhomogeneous distribution of excitation energies, and we calculate the resonance Raman intensities for both the LO and the TO mode. In the bottom panel of Fig. 5, we plot the ratio of the LO and TO intensities at the peak of the inhomogeneously broadened line (solid line).[41] The dephasing rate is dependent on temperature, so we use 80 K to match the experimental conditions, (the experimental data are given by the open circles).[42] We also plot results for which the radius used in the polaron model calculation of S is scaled by a factor of 1.25; this same factor also brought our model calculation into better agreement with the experimental band-gap data plotted in Fig. 3. This gives better agreement with the experimental LO/TO ratio at higher values of R.

VII. DISCUSSION

In our analysis we have treated only the electronic states as confined, and have treated the lattice as expandable into plane waves. The following, semi-classical argument shows that this probably suffices. What we are interested in is the total energy deposited into a finite sized dielectric. Now, if we had a sphere embedded in a larger dielectric which had identical mechanical properties but different electrical properties, we could compute the coupling of the lattice to the confined electronic states using bulk plane waves. We would then find that a number of plane wave modes are displaced according to $F(k)$. Fourier transformation of $F(k)$, leads to $\Delta(r)$, which is the real space deformation of the lattice. $PE(r)$, the potential energy density stored in the lattice, is then given by $\Delta(r)^2/2$ and the total energy stored in the lattice is the integral of $PE(r)$ over space. Our semi-classical approximation is to divide the dielectric, and hence the integral, into two regions:

$$V=\int_0^R PE(\mathbf{r})d\mathbf{r}+\int_R^\infty PE(\mathbf{r})d\mathbf{r}, \tag{47}$$

and to only consider the contributions from the first integral. In practice, we have found that the contribution of the second term is negligible. What this approximation amounts to is a neglect of the detailed boundary conditions of the sphere. The fact that the second term in the integral does not contribute implies that the displacement is not very large near the boundaries.

A second issue concerns the ability of our model to calculate the electronic level structure. Comparison of the measured value of $S=0.08$ for 29 Å radius crystallites indicated that the calculated LO mode couplings are still about a factor of $\sim$3 too low.[28] This is improved somewhat if the radius for the polaron calculation is rescaled by a factor of 1.25. Inspection of Fig. 3 shows that the calculated energy levels give better agreement with the experimental results when the radius is rescaled by a factor of 1.25. This suggests that the calculated energy spacings might be too large, causing both Raman models to have a reduced intensity. In the polaron method, the information about the ordering of energy levels is contained within two parameters, m_e, and m_h. This is a considerable simplification, since we are ignoring both the effect of the light hole band (probably not important in this context, as its effective mass is small) and the highly nonparabolic nature of the conduction band. In reality the electron has a size-dependent effective mass which makes the S_{LO} vs R curve increase more rapidly. Similarly, our ansatz form, Eq. (36), maximizes the phonon overlap (by assuming spherical polarons) whereas the polarization cloud that accompanies isolated charge carriers in the bulk is flattened along the axis of motion.[11,43] This too would lead to a much faster increase with R. To account for both of these effects on the polaron, it would be necessary to completely implement the perturbation method described at the beginning of Sec. IV. In light of these effects, a shift of the radius scaling by a factor of 1.25 is quite reasonable.

There is also the issue of the lifetime. The phonon mode contributions to dephasing rate scale as $1/R^{5/2}$ and thus ''turn on'' quite rapidly with decreasing R. They are responsible for much of the decrease in the LO/TO ratio as the size is decreased. In larger sizes, there are other contributions to the dephasing in nanocrystals which were not included,[38] and thus the dephasing rate is probably underestimated. This would tend to lead to a more gentle increase of the LO/TO ratio with increasing R, consistent with the experimental data.

A final issue is the effect of ionization of the crystallites on the resonance Raman spectrum. Several experiments have demonstrated that within a dispersion of semiconductor crystallites embedded within a matrix which are subjected to CW irradiation there exists a steady state population of ionized crystallites.[44,45] These arise as a result of Auger processes that occur following the absorption of a photon by an optically excited crystallite. While such occurrences are rare, the liberated electron can have very long residence time in the matrix (μs-s), and a significant population of ionized crystallites can be present. Within our model, the presence of an additional charge should not extensively modify the polaron effects with the crystallite, but should lead to a significant increase of the coupling due to the static term [Eq. (29)]. Nomura and Kobayshi have calculated the degree of coupling to the LO modes and the transition dipole moment for a model case of an additional point charge at the center of a

spherical nanocrystal.[15] They found that while the lowest state was bleached, other states had both significant oscillator strength, and increased coupling to the LO modes (about an order of magnitude larger than a nonionized crystallite). Thus the presence of ionized crystallites leads to an increase in the LO intensity, and this would provide a convienent explanation of the remaining discrepancy between our model calculation and the experimental data. There is an additional experimental consequence: The Jahn–Teller theorem guarantees that overall symmetry of the crystallite following ionization cannot be spherical (or even tetrahedral). As a result whether the excess charge is solvated within the crystallite (leading to a large Jahn–Teller effect) or on the surface, the electronic Hamiltonian of the ionized crystallite can have, at most, C_{3v} symmetry. This has a dramatic effect on the polarization properties of the LO mode peak. For a nonionized tetrahedral crystallite the depolarization ratio should be 0 (Sec. II), but for an ionized crystallite the depolarization ratio for the LO modes can have values up to $\frac{1}{3}$.[46] Since the steady state population of ionized crystallites varies linearly in the intensity of the laser,[45] not only should the intensity of LO mode depend on the excitation power, but also its polarization behavior. The calculation of these effects would require the marriage of the methodology found in this paper along with real space techniques for calculation of the wave functions in the presence arbitrary charge dist- ributions.[47]

VIII. CONCLUSIONS

We have presented a set of calculations to describe the size dependence of the resonance Raman cross section in semiconductor nanocrystals. We find that the two different modes which are distinguishable in a Raman experiment have two different origins which are readily visualized. The TO mode intensity results from the distortion of the local bonding geometry which occurs when an optical phonon is excited. Based on previous theories and our own analysis, we predict that in the absence of lifetime effects, the scattering cross section of these modes varies linearly in R and the scattering is depolarized. The LO mode coupling results from the electric fields that are generated upon excitation of an optical phonon. The LO mode should exhibit polarized scattering and an increase in Raman intensity with increasing R. For the experimentally observed LO/TO ratio vs R the models reproduce the qualitative nature of the curve, and the ratio of the two scattering channels. However, the estimate of the coupling strengths is still too low. Nonetheless, the overall agreement is encouraging, and lends support to the description of the physical nature of the problem.

ACKNOWLEDGMENTS

The experimental data discussed here were obtained with the support of U.S. Department of Energy under Contract No. DE-AC03-76SF00098 and by the Office of Navel Research, Order No. N00014-95-F-0099. The theoretical calculations were supported by a NSF-NYI grant. J.R.H. gratefully acknowledges the David and Lucile Packard Foundation for their support.

[1] For a recent review, see A. P. Alivisatos, J. Phys. Chem. **100**, 13 226 (1996), and references therein.
[2] R. Rossetti, S. Nakahara, and L. E. Brus, J. Chem. Phys. **79**, 1086 (1983); A. P. Alivisatos, T. D. Harris, P. J. Carroll, M. L. Steigerwald, and L. E. Brus, *ibid.* **90**, 3463 (1989).
[3] J. J. Shiang, S. H. Risbud, and A. P. Alivisatos, J. Chem. Phys. **98**, 8432 (1993).
[4] A. Tanaka, S. Onari, and T. Arai, Phys. Rev. B. **47**, 1237 (1993)
[5] M. C. Klein, F. Hache, D. Ricard, and C. Flyzanis, Phys. Rev. B **42**, 11123 (1990).
[6] O. I. Micic, J. R. Sprague, C. J. Curtis, K. M. Jones, and A. Nozik, J. Phys. Chem. **98**, 4966 (1994).
[7] A. A. Guzelian J. E. B. Katari A. V. Kandavanich U. Banin, A. P. Alivisatos, R. Wolters, C. C. Arnold, and J. R. Heath J. Phys. Chem. **100**, 7212 (1996).
[8] W. A. Harrison, *Electronic Structure and the Properties of Solids* (Dover, New York, 1989).
[9] W. Potz and P. Vogl, Phys. Rev. B **24**, 2025 (1981).
[10] B. J. Schartz and P. J. Rossky, J. Mol. Liq. **65**, 23 (1995).
[11] T. D. Lee, F. E. Low, and D. Pines, Phys. Rev. **90**, 297 (1953).
[12] Using a value of $m_h = 1.2$ obtained from the data in Table I.
[13] J. Pollman and H. Buttner, Phys. Rev. B **16**, 4480 (1977).
[14] R. Ruppin and R. Englman, Rep. Prog. Phys. **33**, 149 (1970).
[15] S. Nomura and T. Kobayashi, Phys. Rev. B **45**, 1305 (1992).
[16] E. Roca, C. Trallero-Giner, and M. Cardona, Phys. Rev. B **49**, 13 704 (1994).
[17] O. S. Mortesen and S. Hassing, Adv. Infrared Raman Spectrosc. **6**, 1 (1980).
[18] R. Ruppin, J. Phys. C **18**, 2583 (1985).
[19] N. A. Hill and K. B. Whaley, Chem. Phys. **210**, 117 (1996); N. A. Hill, and K. B. Whaley, J. Chem. Phys. **100**, 2831 (1994).
[20] A. I. Ekimov, F. Hache, M. C. Schanne-Klein, D. Ricard, C. Flyzanis, I. A. Kudryavtsev, T. V. Yazeva, A. V. Rodina, and A. L. Efros, J. Opt Soc. B **10**, 100 (1993).
[21] P. C. Sercel and K. J. Vahala, Phys. Rev. B **42**, 3960 (1990).
[22] J. B. Xia, Phys. Rev. B **40**, 8500 (1989).
[23] D. J. Norris, A. A. Sacra, C. B. Murray, and M. G. Bawendi, Phys. Rev. Lett. **72**, 2612 (1994); D. J. Norris, M. M. Kuno M. G. Bawendi, Al. L. Efros, and M. Rosen, *ibid.* **75**, 3728 (1995).
[24] A. Baldereshi and N. Lipari, Phys. Rev. B **8**, 2969 (1973); A. Baldereschi and N. O. Lipari, *ibid.* **9**, 1525 (1974).
[25] P. Vogl, H. Hjalmarson, and J. D. Dow, J. Phys. Chem. Solids, **44**, 365 (1983).
[26] S. Nomura and T. Kobayashi, Solid, State Commun. **82**, 335 (1992).
[27] T. Takagahara, Phys. Rev. Lett. **71**, 3578 (1993).
[28] U. Banin, G. Cerullo, A. A. Guzelian, C. J. Bardeen, A. P. Alivisatos, and C. V. Shank, Phys. Rev. B **55**, 7059 (1997).
[29] A. C. Albrecht, J. Chem. Phys. **34**, 1476 (1961).
[30] M. Cardona, in *Light Scattering in Solids II*, edited by M. Cardona and G. Guntherodt (Springer-Verlag, Berlin 1982), p. 121.
[31] A. B. Myers and R. A. Mathies, in *Biological Applications of Raman Scattering* (Wiley, New York, 1987), Vol. 2, p. 1.
[32] D. J. Tannor and E. J. Heller, J. Chem. Phys. **77**, 202 (1982); S. Ling, D. G. Imre, and E. J. Heller, J. Phys. Chem. **93**, 7107 (1989).
[33] R. A. Harris, R. A. Mathies, and W. T. Pollard, J. Chem. Phys. **85**, 3744 (1986).
[34] A. K. Sood, J. Menedez, M. Cardona, and K. Ploog, Phys. Rev. Lett. **54**, 2111 (1985).
[35] C. Kittel, *Quantum Theory of Solids* (Wiley, New York, 1987).
[36] Al. L. Efros, A. I. Ekimov, F. Kozlowski, V. Petrov-Koch, H. Smidbar, and A. Shumilov, Solid State Commun. **78**, 853 (1991).
[37] R. C. C. Leite, J. F. Scott, and T. C. Damen, Phys. Rev. Lett. **22**, 780 (1969).
[38] D. M. Mittleman, R. W. Schoenlein, J. J. Shiang, V. L. Colvin, A. P. Alivisatos, and C. V. Shank, Phys. Rev. B. **49**, 14 435 (1994).
[39] H. Haken, in *Polarons and Excitons*, edited by C. G. Kuper and G. D. Whitfield (Oliver and Boyd, Edinburgh, 1963), p. 302.
[40] A. P. Alivisatos, A. L. Harris, N. J. Levinos, M. L. Steigerwald, and L. E. Brus, J. Chem. Phys. **89**, 4001 (1988).
[41] We assume an inhomgenous broadening of 150 meV, but provided a sufficiently large value is chosen, the calculated results are do not depend on this parameter.
[42] R. H. Wolters, Thesis, University of California at Los Angeles, 1997.

[43] E. O. Kane, Phys. Rev. B **18**, 6849 (1978).
[44] D. I. Chepic, Al. L. Efros, A. I. Ekimov, M. G. Ivanov, V. A. Kharchenko, I. A. Kuriavsev, and T. V. Yazeva, J. Lumin. **47**, 113 (1990).
[45] M. Nirmal, B. O. Dabbousi, M. G. Bawendi, J. J. Macklin, J. K. Trautman, T. D. Harris, and L. E. Brus, Nature **383**, 802 (1996).
[46] J. J. Shiang, A. V. Kandavanich, and A. P. Alivisatos, J. Phys. Chem. **99**, 17418 (1995).
[47] J. J. Shiang, Thesis, University of California at Berkeley, 1994.
[48] D. Bimberg, K. Hess K, N. O. Lipari., J. U. Fischbach, and M. Altarelli, Physica **89 B**, 139 (1977).
[49] Landolt-Bornstein, K. H. Hellwege, editor in chief, Group III, Vol. 17, *Semiconductors*, Subvol. a (Springer-Verlag, Berlin, 1982), pp. 281–297.